

Interplay between disorder and topology in Thouless pumping on a superconducting quantum processor

Received: 4 March 2024

Accepted: 9 December 2024

Published online: 02 January 2025

 Check for updates

Yu Liu ^{1,2,13}, Yu-Ran Zhang^{3,13}, Yun-Hao Shi ¹, Tao Liu³, Congwei Lu⁴, Yong-Yi Wang ^{1,2}, Hao Li ¹, Tian-Ming Li^{1,2}, Cheng-Lin Deng^{1,2}, Si-Yun Zhou^{1,2}, Tong Liu ¹, Jia-Chi Zhang^{1,2}, Gui-Han Liang^{1,2}, Zheng-Yang Mei^{1,2}, Wei-Guo Ma ^{1,2}, Hao-Tian Liu^{1,2}, Zheng-He Liu^{1,2}, Chi-Tong Chen⁵, Kaixuan Huang ⁶, Xiaohui Song¹, S. P. Zhao ^{1,2,7}, Ye Tian¹, Zhongcheng Xiang ^{1,2,8} , Dongning Zheng ^{1,2,7,8,9}, Franco Nori ^{10,11,12}, Kai Xu ^{1,2,6,7,8,9}  & Heng Fan ^{1,2,6,7,8,9} 

Topological phases are robust against weak perturbations, but break down when disorder becomes sufficiently strong. However, moderate disorder can also induce topologically nontrivial phases. Thouless pumping, as a (1+1)D counterpart of the integer quantum Hall effect, is one of the simplest manifestations of topology. Here, we report experimental observations of the competition and interplay between Thouless pumping and disorder on a 41-qubit superconducting quantum processor. We improve a Floquet engineering technique to realize cycles of adiabatic pumping by simultaneously varying the on-site potentials and the hopping couplings. We demonstrate Thouless pumping in the presence of disorder and show its breakdown as the strength of disorder increases. Moreover, we observe two types of topological pumping that are induced by on-site potential disorder and hopping disorder, respectively. In particular, an intrinsic topological pump that is induced by quasi-periodic hopping disorder has never been experimentally realized before. Our highly controllable system provides a valuable quantum simulating platform for studying various aspects of topological physics in the presence of disorder.

Topology versus disorder provides a diverse landscape for exploration in modern condensed matter physics, ranging from the robustness of topological systems against weak disorder¹ to the classification of symmetry-protected topological phases². One of the most significant

class of topological systems is the Thouless pump^{3,4}, entailing transport of the quantized charge during an adiabatic cyclic evolution of the underlying Hamiltonian^{4,5}. Thouless pumping, as a dynamical version of the integer quantum Hall effect (IQHE)⁶, bridges the quantized

¹Institute of Physics, Chinese Academy of Sciences, Beijing, China. ²School of Physical Sciences, University of Chinese Academy of Sciences, Beijing, China. ³School of Physics and Optoelectronics, South China University of Technology, Guangzhou, China. ⁴Department of Physics, Applied Optics Beijing Area Major Laboratory, Beijing Normal University, Beijing, China. ⁵Quantum Science Center for Guangdong-Hong Kong-Macao Greater Bay Area, Shenzhen, Guangdong, China. ⁶Beijing Academy of Quantum Information Sciences, Beijing, China. ⁷Songshan Lake Materials Laboratory, Dongguan, Guangdong, China. ⁸Hefei National Laboratory, Hefei, China. ⁹CAS Center for Excellence in Topological Quantum Computation, UCAS, Beijing, China. ¹⁰Theoretical Quantum Physics Laboratory, Cluster for Pioneering Research, RIKEN, Wako-shi, Saitama, Japan. ¹¹Center for Quantum Computing, RIKEN, Wako-shi, Saitama, Japan. ¹²Physics Department, University of Michigan, Ann Arbor, MI, USA. ¹³These authors contributed equally: Yu Liu, Yu-Ran Zhang. ✉ e-mail: zcxiang@iphy.ac.cn; kaixu@iphy.ac.cn; hfan@iphy.ac.cn

conductance and the topological invariant, known as the Chern number of the occupied energy bands¹⁷. Due to the universality of topological effects, the Thouless pump is not a specific phenomenon occurring in a certain system and is robust against perturbations^{4,5}. These properties make topological pumps a promising platform for designing novel devices with unprecedented functionalities⁵. Thouless pumping has been experimentally demonstrated on different experimental platforms^{8–19}. Especially, the competition and interplay between topology and disorder in a Thouless pump have been attracting growing attention in, e.g., ultra-cold atoms^{20,21}, photonic waveguides²², and mechanical metamaterials²³. These experiments not only demonstrate topological transitions with disorder, but also the breakdown of quantized pumps due to localization caused by disorder^{24,25}.

To exploit disorder rather than to eliminate it, we experimentally investigate Thouless pumping induced by disorder on a 41-qubit superconducting processor. Since it is challenging to precisely control the adiabatic cyclic evolution of a multi-qubit system with disorder, we employ a Floquet engineering technique^{26–28} to realize Thouless pumping by simultaneously varying the on-site potentials and hopping strengths²⁹. We experimentally demonstrate bulk topological pumping during different pumping trajectories in the clean limit. We also observe the breakdown of quantized pumping, when the strength of the random on-site potential disorder increases. For a topologically trivial double-loop pumping trajectory, we observe topological pumping induced by the on-site disorder of a uniform random distribution. Moreover, we experimentally demonstrate emergent topological pumping induced by quasi-periodic hopping disorder, which is related to the dynamic version of topological Anderson insulators (TAI)^{30–35}. Our results will inspire further investigations of topological phases in the presence of disorder on quantum simulating platforms^{36–44}.

Results

System and model

Our experiments are performed on a 1D superconducting processor, named *Chuang-tzu*, consisting of 43 nearest-neighbor-coupled and frequency-tunable transmon qubits²⁸. In our experiments, 41 qubits (Q_j with j varying from 1 to 41) are used, and the system Hamiltonian is written as $\hat{H}_0 = \sum_j [(g_{j,j+1} \hat{a}_j^\dagger \hat{a}_{j+1} + \text{H.c.}) + \omega_j \hat{n}_j]$, where \hat{a}_j^\dagger (\hat{a}_j) denotes the hard-core bosonic creation (annihilation) operator⁴⁵, $\hat{n} = \hat{a}^\dagger \hat{a}$ is the

number operator, and $g_{j,j+1}$ is the nearest-neighbor (NN) hopping strength.

To experimentally demonstrate a disorder-induced pumping process, we simulate the tight-binding Rice-Mele (RM) model with on-site potential disorder or hopping disorder, of which the Hamiltonian can be expressed as⁴⁶:

$$\hat{H}_{\text{RM}}(t) = \sum_{j=1}^{40} \left\{ J + (-)^{j-1} [\delta(t) + W_j] \right\} (\hat{a}_j^\dagger \hat{a}_{j+1} + \text{H.c.}) + \sum_{j=1}^{41} (-)^{j-1} [\Delta(t) + V_j] \hat{n}_j. \quad (1)$$

Here, $J \pm [\delta(t) + W_j]$ denote the NN hopping strengths with disorder W_j , $\pm [\Delta(t) + V_j]$ denote the staggered on-site potential with disorder V_j , and $\Delta(t)$ and $\delta(t)$ are periodic with the period T . When $\Delta(t) = 0$, the RM model reduces to the Su-Shrieffer-Heeger (SSH) model⁴⁷ in the clean limit. Furthermore, to realize the adiabatic cyclic evolution of the RM Hamiltonian (1), we develop a Floquet engineering technique to change the dynamical parameters $\delta(t)$ and $\Delta(t)$ adiabatically during a closed trajectory in a δ - Δ space (Fig. 1b). More details are discussed in the Supplementary Materials²⁹. We realize the pumping process with the cyclic modulations of both the amplitude and the center offset of the sine-like waves of Floquet engineering, corresponding to the cyclic variations of the hopping coupling and the on-site potential, respectively, where disorder is also carefully introduced.

Topological invariant and topological pumping

In the clean limit, the continuous RM pumping sequence is periodic in both spatial and temporal dimensions. Under periodic boundary conditions (PBCs), the Bloch wavefunction of the n -th energy band is defined in the k - t Brillouin zone as $|\psi_{k,n}(t)\rangle = e^{ikx} |u_{n,k}(t)\rangle$, and the Chern number is expressed as⁹

$$\nu_n = \frac{1}{2\pi} \int_{\text{FBZ}} dk \int_0^T dt \Omega_n(k, t), \quad (2)$$

where $\Omega_n(k, t) = i(\langle \partial_t u_{n,k} | \partial_k u_{n,k} \rangle - \langle \partial_k u_{n,k} | \partial_t u_{n,k} \rangle)$ denotes the Berry curvature, and FBZ represents the first Brillouin zone. When the system is initially prepared as a Wannier state, filling the n -th band, ν_n relates to

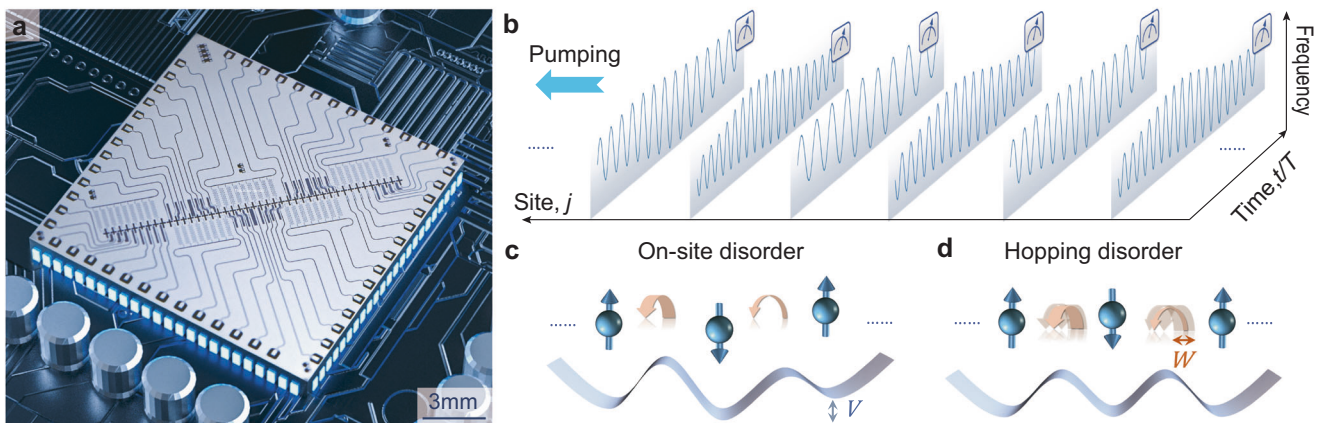


Fig. 1 | Device and pulse sequences. **a** Optical micrograph of the 43-qubit superconducting chip. **b** Schematic of Floquet engineering for the adiabatic cyclic evolution. Pulse sequences in one pumping period are illustrated. The amplitude and the center shift of the Floquet engineering pulse on each qubit are subject to a cyclic modulation, corresponding to the cyclic variations of hopping couplings and on-site potentials, respectively. **c** Schematic diagram of the Rice-Mele (RM) model with on-site potential disorder. The on-site potentials on qubits are staggered, with a random

offset of disorder strength V . The orange curved arrows, representing the couplings, stagger with one large and one small, due to the staggered RM hopping Hamiltonian. **d** Schematic diagram of the RM model in the presence of hopping disorder. The on-site potential is strictly periodic, while the disordered hopping coupling is modulated with disorder strength W . In the clean limit, the on-site potentials (hopping couplings), denoted by the blue spin (orange curved arrows), are staggered with one up (large) and one down (small) due to the staggered RM Hamiltonian.

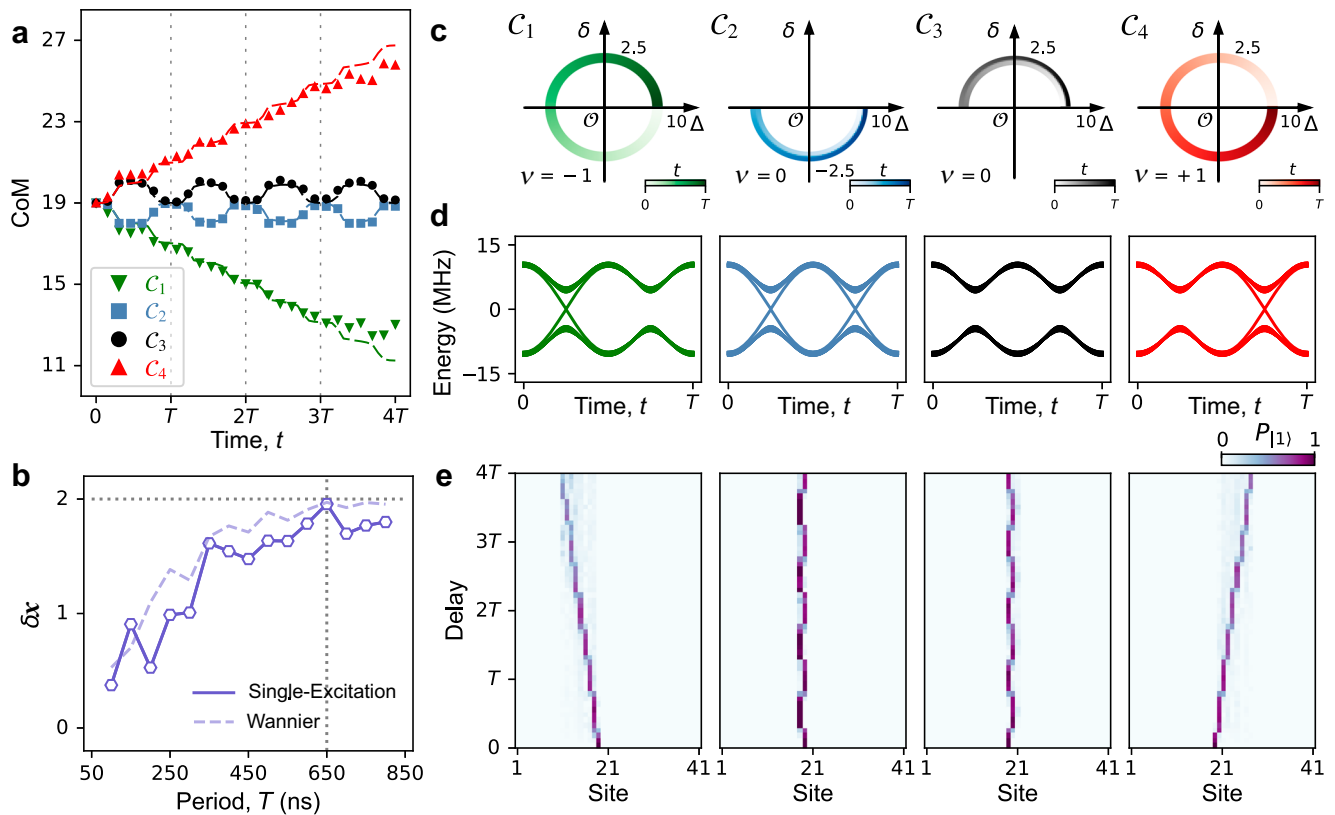


Fig. 2 | Bulk topological pumping for different types of cycles initially with single-excitation states. **a** Displacements of the CoM for four different pumping trajectories C_1 – C_4 as illustrated in (c). Dashed curves represent the numerical results. **b** Displacement of CoM, δx , versus the pumping period T , for C_4 initially with a single-excitation state. When $T = 650$ ns, δx reaches the maximum 1.95(6). The dashed curve shows the numerical results of δx as a function of T , when the initial state is an exact Wannier state. **c** Four different pumping trajectories C_1 – C_4 in the δ – Δ plane. The trajectory C_4 is set as $(\Delta, \delta) = (\Delta_0 \cos 2\pi t/T, \delta_0 \sin 2\pi t/T)$, with

$\Delta_0/2\pi = 10$ MHz, $\delta_0/2\pi = 2.5$ MHz, and $J/2\pi = 2$ MHz. The trajectory C_3 is set as $(\Delta, \delta) = (\Delta_0 \cos 2\pi t/T, \delta_0 \sin 2\pi t/T)$ with the same parameters Δ_0 , δ_0 , and T as C_4 . The trajectory C_1 (C_2) is designed symmetrically flipped about the Δ -axis with C_4 (C_3). The trajectory C_1 and C_4 correspond to the Chern numbers $\nu = \mp 1$, respectively, and C_2 and C_3 lead to topologically trivial pumping. **d** Instantaneous energy spectra of the bulk under open boundary conditions. **e** Experimental data of the populations of all qubits during the adiabatic cyclic evolution within four periods.

the displacement of the center-of-mass (CoM) per pumping cycle δx as

$$\delta x = \nu_n d, \tag{3}$$

with $d = 2$ being the lattice constant⁴⁸.

In our experiments, we engineer the continuous RM model in the clean limit and implement topological pumping by periodically modulating δ and Δ that sketch a closed trajectory in the δ – Δ space within a period T . The initial state is prepared as a single-excitation state, having an overlap of over 0.99 with the exact Wannier state²⁹, by exciting one qubit closest to the middle, i.e., Q_{19} . During the pumping procedure, we measure the population of each qubit $P_{|j\rangle} \equiv \langle \hat{n}_j \rangle$, with which the CoM can be calculated as $\bar{x} \equiv \sum_j j \langle \hat{n}_j \rangle$. The experimental results of the shift of the CoM after four pumping cycles are shown in Fig. 2 for four distinct pumping trajectories C_1 – C_4 (Fig. 2c), respectively. The period is carefully chosen as $T = 650$ ns, when the mean δx achieves its maximum 1.95(6) (Fig. 2b). Here, the slight oscillation of δx for $T > 650$ ns originates from the difference between the single-excitation state and the exact Wannier state. Quantized charge pumping is observed for topologically nontrivial pumping trajectories C_1 and C_4 around the gapless point $(\Delta, \delta) = (0, 0)$, corresponding to the Chern numbers ∓ 1 , respectively. Moreover, topologically trivial pumping is probed for C_2 and C_3 with zero Chern number. The corresponding energy bands under open boundary conditions are shown in Fig. 2d for C_1 – C_4 , respectively, which could be measured by a dynamical spectroscopic technique²⁸. The deviation for $t > 3T$, between the experimental and numerical

results in Fig. 2a, are due to dephasing²⁹. Adiabatic time evolutions for a pumped excitation during pumping trajectories C_1 – C_4 are shown in Fig. 2e. In addition, we experimentally monitor the double-excitation pumps for different trajectories²⁹, which are shown in Fig. 3. The experimental results are similar to the single-excitation cases, as the system is in the hard-core limit⁴⁵. Since the pumps of excitations initially prepared at odd and even sites have opposite winding numbers⁴⁸, no quantized pumping is observed for the topologically nontrivial pumping trajectory C_4 , when the parity of the initial excitation sites is different (Fig. 3d).

Pumping in the presence of on-site disorder

Next, we investigate the effects of on-site potential disorder on topological pumping. Figure 4a shows the displacement of the CoM for a forward pump, with respect to the pumping trajectory C_{out} (inset of Fig. 4c), versus the on-site disorder strength $V/2\pi$. Here, the on-site potential disorder V_j on each qubit satisfies a uniform random distribution in the range $[-V, V]$. The experimental results demonstrate that quantized pumping persists for $V/\Delta_0 \lesssim 1$, but degrades as the displacement of the CoM per pumping cycle δx decays to zero for $V \gtrsim 3\Delta_0$. In addition, we numerically calculate the pumping amounts of charge over one cycle, i.e.,

$$\Delta Q = d \int_0^T dt \langle \psi(t) | \hat{J}(t) | \psi(t) \rangle, \tag{4}$$

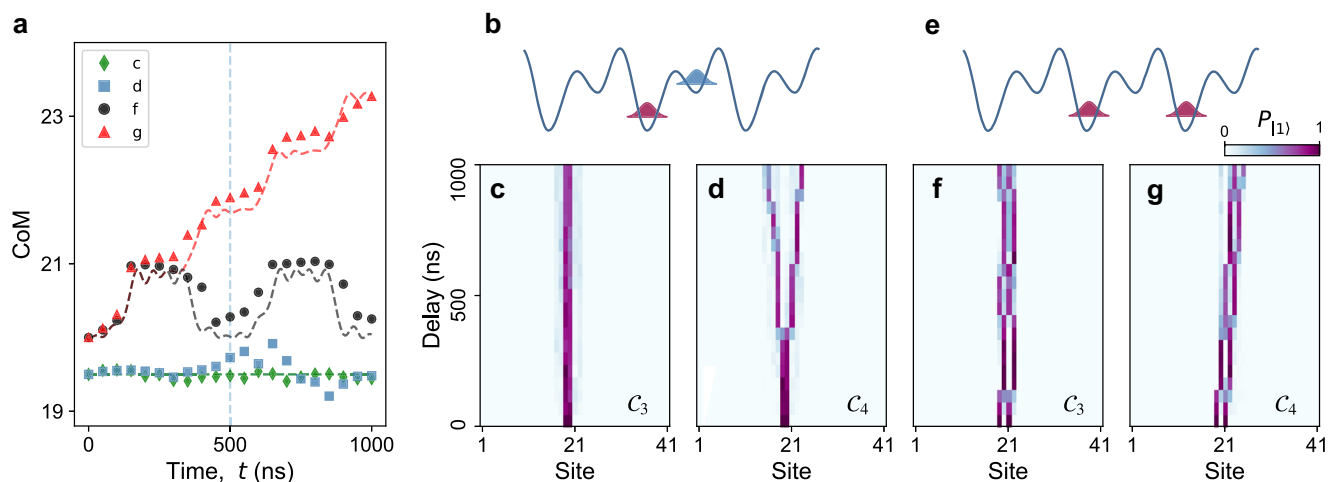


Fig. 3 | Topological pumping for different types of cycles which initially have double-excitation states. **a** Displacements of the CoM for different pumping protocols as shown in **(c, d, f, g)**, where the dashed curves represent the numerical results. **b** Schematic diagram of lattice potentials with the initial excitations prepared at two nearest-neighbor sites, i.e., Q_{19} and Q_{20} . **c, d** Experimental data of the population of all qubits during the adiabatic cyclic evolution within two periods for

the trajectory C_3 and C_4 , respectively. **e** Schematic diagram of lattice potential with the initial state prepared by exciting two next-neighbor sites, i.e., Q_{19} and Q_{21} . Adiabatic time evolutions of the populations of all qubits within two periods for the pumping trajectories C_3 and C_4 are shown in **(f, g)**. The evolution period for double-excitation pumping is 500 ns.

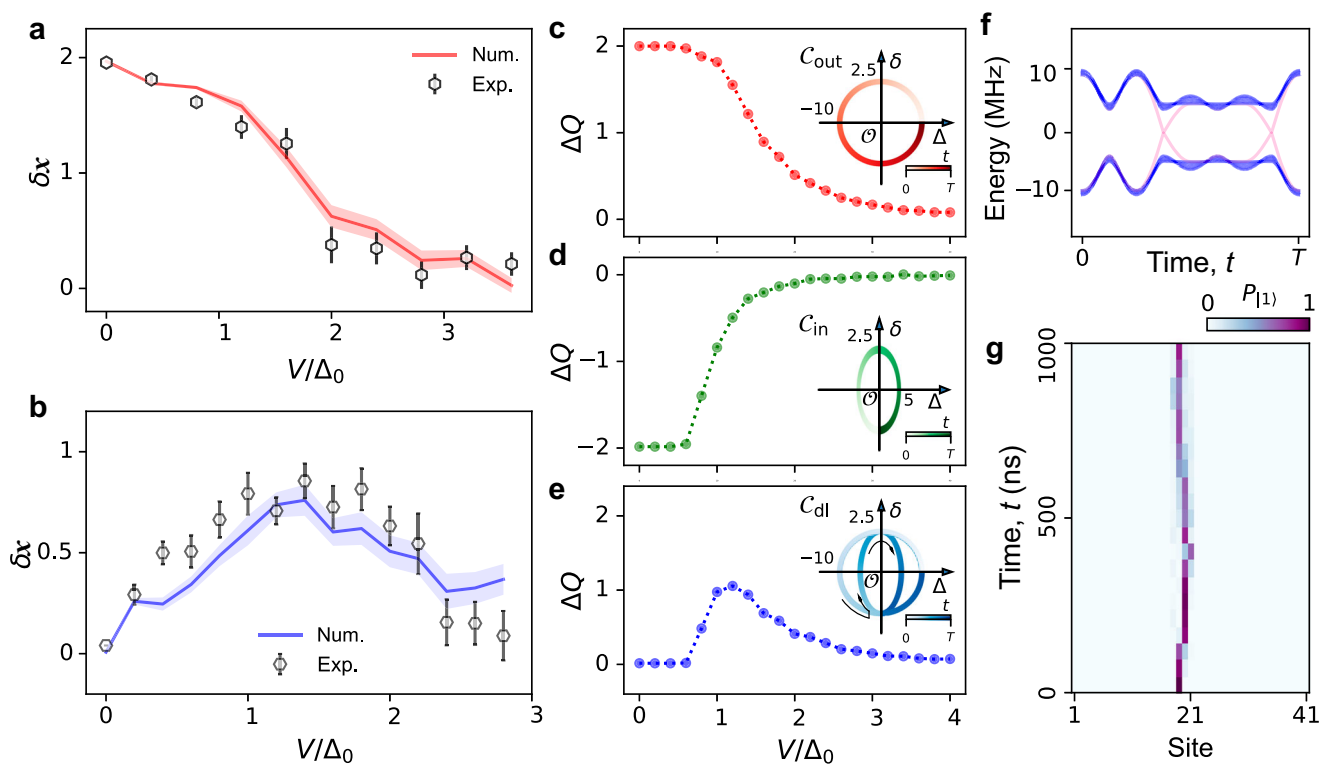


Fig. 4 | Pumping with on-site disorder. **a** Experimental data of the displacement of the CoM δx for 2 pumping periods against the on-site potential disorder strength V divided by $\Delta_0/2\pi = 10$ MHz during the pumping trajectory C_{out} as plotted in the inset of **(c)**. On-site potential disorder V_j follows a uniform random distribution within the range $[-V, V]$. The red solid curve represents the mean numerical results, and the error bars represent the standard error of the experimental (numerical) results with 30 (100) configurations of disorder. **b** Experimental data of δx versus V during a double-loop pumping trajectory C_{dl} as shown in the inset of **(e)**. **c** Numerical results of the charge pumped per cycle ΔQ versus V during the outer-loop pumping

trajectory C_{out} . **d** Numerical results of ΔQ versus V during the inner-loop pumping trajectory C_{in} . **e** ΔQ for double-loop pumping C_{dl} , which is obtained by summing the results of outer- and inner-loop pumping. **f** Bulk energy band for double-loop pumping under open boundary conditions. Darker colors imply higher state density. **g** Experimental data of the average populations of all qubits during the adiabatic cyclic evolution for double-loop pumping over 30 independent disorder configurations. The period of both the outer- and the inner-loop pumping is set as 500 ns.

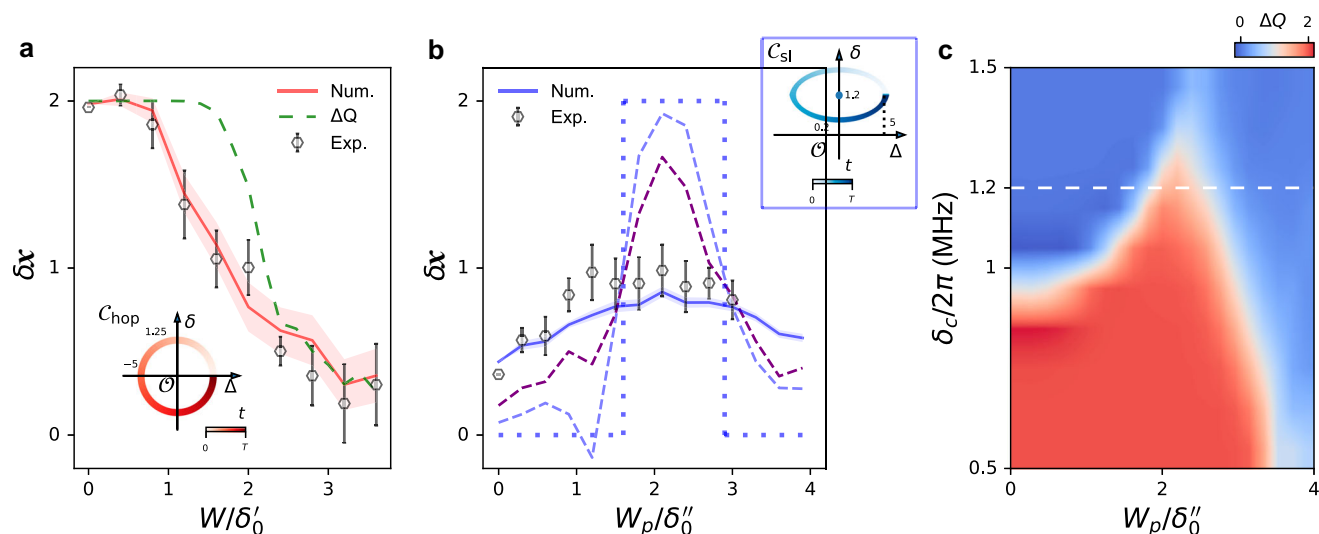


Fig. 5 | Pumping with hopping disorder. **a** Experimental data for the displacement of the CoM δx for one pumping period versus the random hopping disorder strength W during the pumping trajectory C_{hop} as shown in the inset. The red solid and green dashed curves plot the numerical results of δx and ΔQ , respectively. **b** Experimental data of δx against the quasi-periodic disorder strength W_p during the pumping trajectory C_{sl} : $(\Delta, \delta) = (\Delta'_0 \cos 2\pi t/T, \delta_c + \delta''_0 \sin 2\pi t/T)$, with $\Delta'_0/2\pi = 5$ MHz, $\delta_c/2\pi = 1.2$ MHz, $\delta''_0/2\pi = 1$ MHz, $T = 1.4$ μs , and $J/2\pi = 1.8$ MHz. The solid blue curve denotes the numerical simulation and the dotted curve shows the

topological index calculated in the thermodynamic limit⁵⁵. The purple (light blue) dashed curve denotes the numerical results using similar experimental parameters but with a longer period 20 μs (80 μs) in a larger system with 200 (800) qubits. Experimental data are averaged over 30 disorder configurations, while the numerical simulation is calculated for 1000 disorder configurations. **c**. Charge pumped per cycle ΔQ versus W_p and δ_c . The white dashed horizontal line shows the TAI-like topological transition of pumping during C_{sl} .

to characterize the interplay between topology and disorder^{24,35} (Fig. 4c–e). Here, the average current density can be expressed as

$$\hat{\mathcal{J}}(t) = i \sum_{j=1}^N [(J + (-1)^{j-1} \delta) \hat{a}_{j+1}^\dagger \hat{a}_j + \text{H.c.}] / N, \quad (5)$$

and $|\psi(t)\rangle$ is the time evolved state initially with a half-filling ground state of the system, and $i = \sqrt{-1}$. As shown in Fig. 4c, ΔQ versus V has a similar behavior as the experimental results of δx . The slight reduction of ΔQ when $V/\Delta_0 \lesssim 1$ results from the use of a single-excitation initial state instead of an exact Wannier state. The breakdown of quantized pumping can be understood due to the closing band gap, leading to the Landau-Zener transition^{4,49}. The gap closes when $V \approx \Delta_0$ ²⁹, which conforms to the experimental observations of δx . Thus, the breakdown may be due to localization of single-particle Floquet states instead of that of instantaneous eigenstates, for which localization occurs for any non-zero disorder strength²⁴.

In addition, we demonstrate a pumping procedure following a double-loop pumping trajectory, C_{dl} , to study topological pumping that is induced by random on-site disorder. As plotted in the inset of Fig. 4e, this closed pumping trajectory is composed of an outer loop C_{out} (inset of Fig. 4c) and an inner loop C_{in} (inset of Fig. 4d). Since along C_{out} and C_{in} , the system evolves into a parameter plane with opposite Chern numbers as $\nu_{\text{out}} + \nu_{\text{in}} = 0$. However, as the on-site disorder strength V increases, the gapless regime appears around the origin \mathcal{O} along the Δ -axis. When $0.5 \lesssim V/\Delta_0 \lesssim 2$, the inner loop cannot encircle the whole gapless regime and no topological pumping phenomenon occurs, while the outer loop remains nontrivial with $\nu_{\text{out}} = +1$. Thus, with a moderate disorder strength, we observe nontrivial pumping induced by the on-site disorder with $\delta x \neq 0$ (Fig. 4b). However, a quantized disorder-induced pump can hardly be realized, since quantized transport requires trajectory parameters to be finely tuned to combine the effects of the trivial inner and outer trajectories²⁰. As the disorder strength increases further to $V/\Delta_0 \gtrsim 2.5$, pumping becomes trivial, since no topological pumping exists for the outer loop. The increase of δx in

the region $0 \lesssim V/\Delta_0 \lesssim 0.7$ is also due to the discrepancy between the single-excitation and Wannier initial states.

Pumping with hopping disorder

Next, we experimentally investigate topological pumping in the presence of hopping disorder. We choose a trivial pumping trajectory C_{hop} : $(\Delta, \delta) = (\Delta'_0 \cos 2\pi t/T, \delta'_0 \sin 2\pi t/T)$, with $\Delta'_0/2\pi = 5$ MHz, $\delta'_0/2\pi = 1.25$ MHz, $J/2\pi = 1$ MHz, and $T = 1.3$ μs (inset of Fig. 5a). First, we consider uniform random hopping disorder within the range $[-W, W]$. The experimental results, shown in Fig. 5a, are similar to the ones with on-site potential disorder as shown in Fig. 4a, where the increase of the disorder strength leads to the decrease of δx . However, the decay of δx obeys a distinct law from the on-site potential disorder case⁵⁰, when the 1D system tends to the localization phase. A non-adiabatic evolution could cause the breakdown of quantized pumping with a smaller disorder strength, which is verified by comparing the charge pumped with a longer period with the transition point at $W/\delta_0 \approx 1$ ²⁹.

Recently, it has been suggested that quasi-periodic hopping disorder would lead to exotic topological phenomena⁵¹. Moreover, as the gap would reopen, applying quasi-periodic hopping disorder may intrinsically induce topological pumping, which can hardly be realized by introducing random hopping disorder^{29,35}. Here, we consider a topologically trivial single-loop pumping trajectory with its center being biased away from the gapless point \mathcal{O} (origin of Δ - δ plane), i.e., C_{sl} : $(\Delta, \delta) = (\Delta'_0 \cos 2\pi t/T, \delta_c + \delta''_0 \sin 2\pi t/T)$ with $\Delta'_0/2\pi = 5$ MHz, $\delta_c/2\pi = 1.2$ MHz, $\delta''_0/2\pi = 1$ MHz, $T = 1.4$ μs , and $J/2\pi = 1.8$ MHz (inset of Fig. 5b). Quasi-periodic hopping disorder, $W_j = W_p \cos(2\pi \alpha j + \beta)$, is introduced on each even qubit, with $\alpha = (\sqrt{5} - 1)/2$ being irrational and $\beta \in [-\pi, \pi)$ being an arbitrary random phase offset. As the disorder strength W_p increases, the gapless point would appear inside the pumping loop³⁵, and nontrivial pumping could be observed (see the theoretical predictions in Fig. 5b). Though under insufficient adiabaticity, we demonstrate the observation of signatures consistent with topological pumping induced by quasi-periodic hopping disorder, which leads to nonzero in the clean limit. Theoretically, with an extremely long evolution period, e.g., 20 μs and 80 μs , as shown in

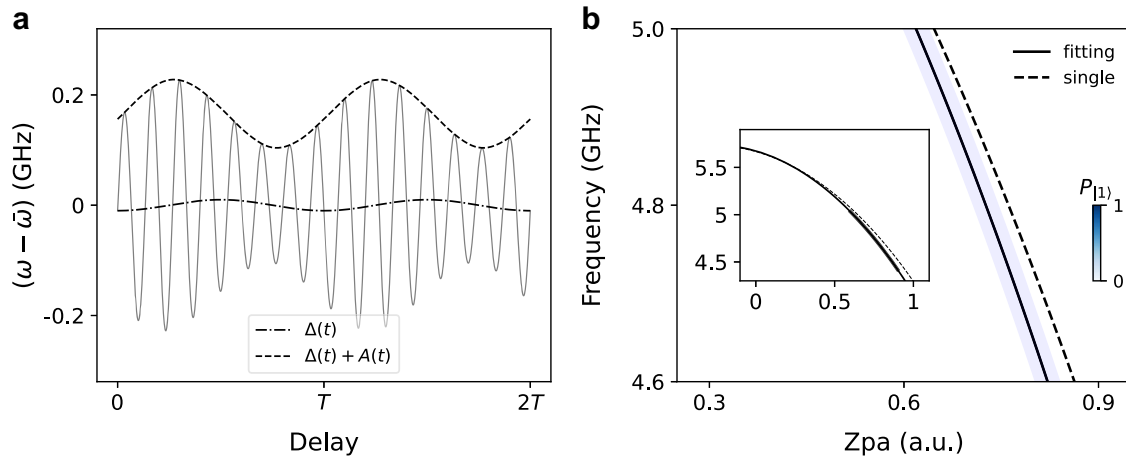


Fig. 6 | Pulse sequence. **a** Schematic of the qubit frequency. The frequency is manipulated as amplitude-modulated sinusoidal wave with a moving center. **b** Multi-qubit spectroscopy measurement. The dashed line represents the mapping from Z pulse amplitude (Zpa) to qubit frequency obtained by single-qubit

spectroscopy. The solid line shows fitting result from the multi-qubit spectroscopy segment. Due to crosstalk, the dashed line deviates from the actual mapping when tuning all qubits to their work points, indicated by curves in the inset.

Fig. 5b, non-adiabatic effects can be suppressed. Moreover, this non-trivial pumping phenomenon could also be viewed as a dynamical version of TAls^{32,33}, as the numerical results of ΔQ in Fig. 5c indicates the existence of TAl-like topological transitions.

Discussion

We experimentally investigated the competition and interplay between topology and disorder in topological pumping on a 41-qubit superconducting processor. Furthermore, we demonstrated disorder-induced topological pumping which was induced by either on-site random disorder or quasi-periodic hopping disorder. In addition, we experimentally studied the robustness and the breakdown of a Thouless pump as the disorder strength increases. Note that these experimental results were obtained by extending the multi-qubit Floquet engineering technique to the adiabatic evolution regime, which would be helpful in exploring various topological phenomena induced by disorder.

Methods

Floquet engineering for adiabatic systems

In our experiments, we employ an extended Floquet engineering technique with the high-frequency expansion⁵² to realize the RM model, which is an effective approach to modulate hopping strengths between qubits. Since the simultaneous changes of on-site potentials and hopping strengths are inherently necessary, we extended Floquet engineering for adiabatic systems, by carefully introducing two restrictions: the adiabatic condition and the Nyquist condition. Specifically, we manipulate the Z pulse to tune the j -th qubit frequency according to

$$\omega_j(t) = \bar{\omega} + \Delta_j(t) + A_j(t) \sin(\mu t + \varphi_0), \quad (6)$$

where $\bar{\omega}$ is the average frequency, A_j , μ , and φ_0 denote modulation amplitude, frequency, and phase, respectively, and Δ_j is the j -th on-site potential. Experimentally, we set $\bar{\omega}/2\pi = 4.8$ GHz, and $\mu/2\pi = 80$ MHz for all qubits, and a schematic of the qubit frequency is plotted in Fig. 6a. To realize the high-frequency expansion, the modulation frequency should be higher than the simulated frequency regime for fulfilling the adiabatic condition, and the effective Hamiltonian contains a series of frequency bands. The Nyquist condition requires that the variation range of the difference between two neighbor on-site potentials should be lower than half the modulation frequency $\mu/2$. This can avoid any overlap between different frequency bands,

resulting in an effective simulation of the target time-evolved Hamiltonian under the rotating wave approximation.

By introducing the superconducting quantum interference device (SQUID) into the transmon qubit, the qubit is frequency-tunable, and the relationship between the qubit frequency ω and the flux Φ_e , entering the loop of SQUID⁵³, is

$$\omega = \sqrt{8E_J E_C |\cos(\pi\Phi_e/\Phi_0)|} - E_C, \quad (7)$$

where E_J denotes the Josephson energy when $\Phi_e = 0$, E_C is the charging energy, and Φ_0 is the flux quantum. For weak magnetic fields, Φ_e is linearly related to the experimental Z pulse amplitude (Zpa), i.e., $\pi\Phi_e/\Phi_0 = kV_z + b$. These parameters can be extracted by the single-qubit spectroscopy measurement experiments. However, the parameters obtained in this way would be inaccurate due to the unavoidable crosstalk after tuning all qubits to their idle points. Thus, we apply the multi-qubit spectroscopy measurements in the range near the working points or the average frequency $\bar{\omega} \sim 4.8$ GHz, see Fig. 6b. Then, we fit the relationship in Eq. (7) using this small segment of the spectroscopy data, which exhibits a linear correlation. Although under-fitting seems to occur, we could achieve the desired results by fixing the known parameters insensitive to the crosstalk, such as E_C and the sweet points of qubits. The inset of Fig. 6b shows the optimized mapping from Zpa to the qubit frequency, which differs from single-qubit fitting result.

Combining Eqs. (6) and (7), we can obtain the Z pulse waveform, applied on the j -th qubit V_j^z , as $V_j^z = \frac{1}{k_j} \arccos \left[\pm \frac{(\bar{\omega} + \Delta_j(t) + A_j(t) \sin(\mu t + \varphi_0) + E_C^j)^2}{8E_J^j E_C^j} \right] - \frac{b_j}{k_j}$. Note that $A_j(t)$ is dependent of the modulation amplitude of the nearest qubits $A_{j-1}(t)$ and $A_{j+1}(t)$. In practical operations, we establish a reference amplitude, which is a smooth function, for a specific qubit Q_k . For convenience, we simply set $A_k(t) \equiv 0$, and then, we perform the iterative calculation of Q_k to obtain $A_{k+1}(t)$, $A_{k+2}(t)$, \dots and $A_{k-1}(t)$, $A_{k-2}(t)$, \dots .

Using the method as introduced above, we can engineer a time-dependent Hamiltonian with the simultaneous adjustment of the on-site potentials and the hopping strengths on our superconducting processor with only frequency-tuning capabilities. Numerically, we calculate pumping for the trajectory, C_4 , by evolving the exact RM model as shown in Fig. 7a and the same Hamiltonian, but constructed through Floquet engineering, as shown in Fig. 7b, respectively. The CoM extracted from these two methods coincide very well, see Fig. 7c.

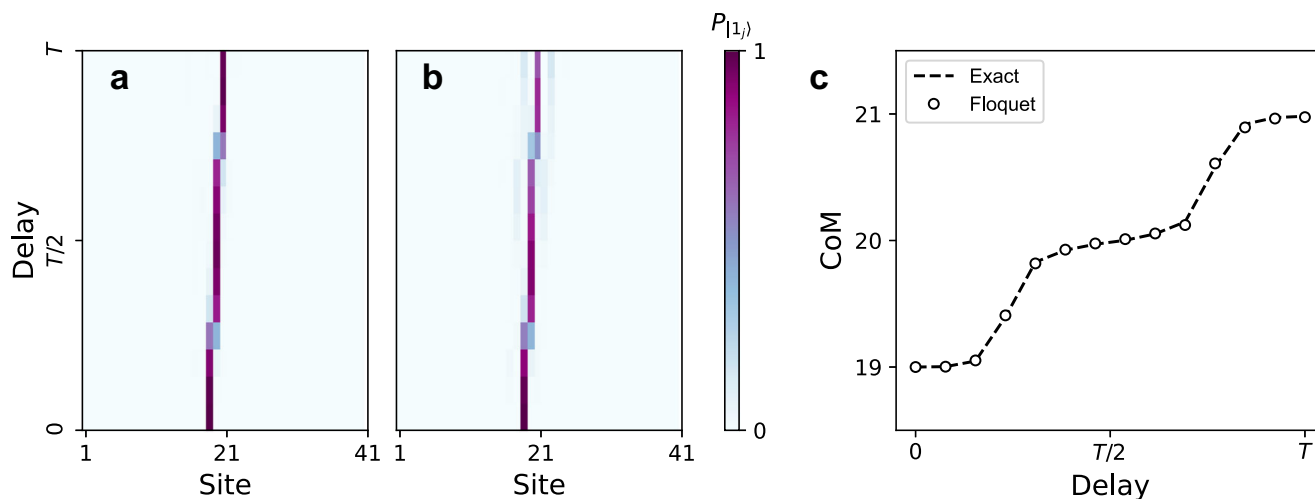


Fig. 7 | Numerical calculation of pumping for C_4 . **a** Numerical results of the time evolution of the initial single-excitation state obtained by evolving the exact Rice-Mele model Hamiltonian over one cycle. **b** Numerical results of the time evolution of the initial single-excitation state obtained by evolving the Rice-Mele model

Hamiltonian constructed through Floquet engineering over one cycle.

c Numerical results of CoM extracted from (a, b). The initial state is chosen as a single-excitation state at the 19-th site, and the modulation frequency μ is set as $\mu/2\pi = 80$ MHz.

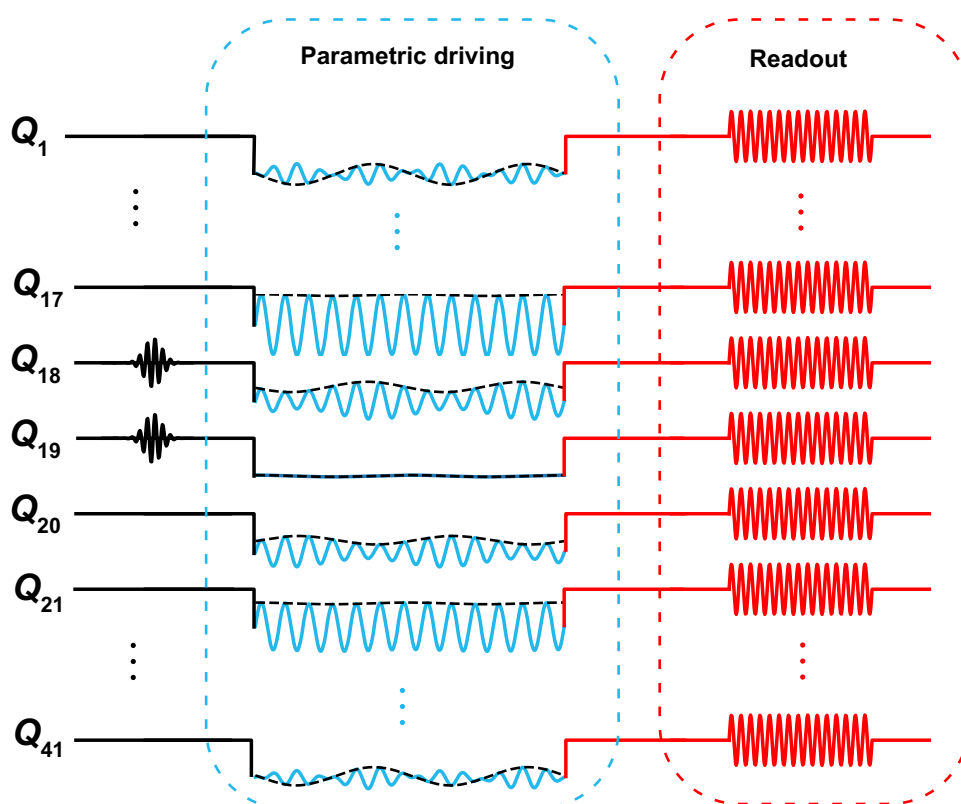


Fig. 8 | Pulse sequence for topological pumping with double excitations. All qubits are initialized at their idle points. Then, Q_{18} and Q_{19} are excited using the Gaussian-like derivative removal by adiabatic gate (DRAG) pulses. Next, all qubits

are driven by performing parametric modulations through their Z-control lines. After a delay time, the parametric driving is turned off, and all qubits are tuned back to their idle points for readouts.

Experimental setup

Our superconducting quantum processor consists of 43 transmon qubits arranged in a 1D array, labeled as Q_1, \dots, Q_{43} , and we used Q_3, \dots, Q_{43} (relabelled as Q_1, \dots, Q_{41}) for the experiments. The qubits are capacitively coupled to their nearby qubits with a mean hopping strength $\bar{g}/2\pi \approx 7.2$ MHz, which suggests that the adjustable range of the effective hopping strengths is from -2.9 MHz to 7.2 MHz. Since the

average anharmonicity is $\bar{U}/2\pi \approx -208$ MHz, with a ratio $|\bar{U}/\bar{g}| \approx 29 \gg 1$, our processor can be regarded as a hard-core bosonic system⁴⁵. The mean energy relaxation time is $21.0 \mu\text{s}$, and the sweet points of qubits are designed to be staggered for the convenience of arranging energy levels, with a mean value of 5.014 GHz.

With all 41 superconducting qubits initialized at their idle points, we prepared the localized initial state using an X gate, as an

approximation to the Wannier state. By using the derivative removal by adiabatic gate (DRAG) theory⁵⁴, the X gate pulse is optimized to minimize the leakage to higher energy levels, achieving an average gate fidelity of 99.2%. Then, the parametric flux modulations are applied on all qubits to engineer the Rice-Mele Hamiltonian, for different pumping experiments. The schematic diagram of the pulse sequence, for the double-excitation experiments as an example, is shown in Fig. 8. After turning off the parametric driving, the qubits are tuned back to their idle points for readout. The states of all qubits can be read out simultaneously through the transmission lines coupled to readout resonators. All qubit probabilities are corrected to eliminate the measurement errors.

Data availability

The source data underlying all figures are available at <https://doi.org/10.6084/m9.figshare.27908871>. Other data are available from the corresponding author upon request.

References

- Moore, J. E. The birth of topological insulators. *Nature* **464**, 194 (2010).
- Qi, X.-L. & Zhang, S.-C. Topological insulators and superconductors. *Rev. Mod. Phys.* **83**, 1057 (2011).
- Thouless, D. J. Quantization of particle transport. *Phys. Rev. B* **27**, 6083 (1983).
- Niu, Q. & Thouless, D. J. Quantised adiabatic charge transport in the presence of substrate disorder and many-body interaction. *J. Phys. A: Math. Gen.* **17**, 2453 (1984).
- Citro, R. & Aidelburger, M. Thouless pumping and topology. *Nat. Rev. Phys.* **5**, 87 (2023).
- Thouless, D. J., Kohmoto, M., Nightingale, M. P. & den Nijs, M. Quantized Hall Conductance in a Two-Dimensional Periodic Potential. *Phys. Rev. Lett.* **49**, 405 (1982).
- Xiao, D., Chang, M.-C. & Niu, Q. Berry phase effects on electronic properties. *Rev. Mod. Phys.* **82**, 1959 (2010).
- Nakajima, S. et al. Topological Thouless pumping of ultracold fermions. *Nat. Phys.* **12**, 296 (2016).
- Lohse, M., Schweizer, C., Zilberberg, O., Aidelburger, M. & Bloch, I. A Thouless quantum pump with ultracold bosonic atoms in an optical superlattice. *Nat. Phys.* **12**, 350 (2016).
- Lohse, M., Schweizer, C., Price, H. M., Zilberberg, O. & Bloch, I. Exploring 4D quantum Hall physics with a 2D topological charge pump. *Nature* **553**, 55 (2018).
- Cheng, W., Prodan, E. & Prodan, C. Experimental Demonstration of Dynamic Topological Pumping across Incommensurate Bilayered Acoustic Metamaterials. *Phys. Rev. Lett.* **125**, 224301 (2020).
- Kao, W., Li, K.-Y., Lin, K.-Y., Gopalakrishnan, S. & Lev, B. L. Topological pumping of a 1D dipolar gas into strongly correlated prethermal states. *Science* **371**, 296 (2021).
- Jürgensen, M., Mukherjee, S. & Rechtsman, M. C. Quantized nonlinear Thouless pumping. *Nature* **596**, 63 (2021).
- Mostaan, N., Grusdt, F. & Goldman, N. Quantized topological pumping of solitons in nonlinear photonics and ultracold atomic mixtures. *Nat. Commun.* **13**, 5997 (2022).
- You, O. et al. Observation of Non-Abelian Thouless Pump. *Phys. Rev. Lett.* **128**, 244302 (2022).
- Xiang, Z.-C. et al. Simulating quantum Hall effects on a superconducting quantum processor. *Nat. Commun.* **14**, 5433 (2023).
- Dreon, D. et al. Self-oscillating pump in a topological dissipative atom-cavity system. *Nature* **608**, 494 (2022).
- Tao, Z. et al. Interaction-induced topological pumping in a solid-state quantum system, <https://arxiv.org/abs/2303.04582>
- Jürgensen, M., Mukherjee, S., Jörg, C. & Rechtsman, M. C. Quantized fractional Thouless pumping of solitons. *Nat. Phys.* **19**, 420 (2023).
- Nakajima, S. et al. Competition and interplay between topology and quasi-periodic disorder in Thouless pumping of ultracold atoms. *Nat. Phys.* **17**, 844 (2021).
- Walter, A.-S. et al. Quantization and its breakdown in a Hubbard-Thouless pump. *Nat. Phys.* **19**, 1471–1475 (2023).
- Jerjan, A., Wang, M., Huang, S., Chen, K. P. & Rechtsman, M. C. Thouless pumping in disordered photonic systems. *Light Sci. Appl.* **9**, 178 (2020).
- Grinberg, I. H. et al. Robust temporal pumping in a magneto-mechanical topological insulator. *Nat. Commun.* **11**, 974 (2020).
- Wauters, M. M., Russomanno, A., Citro, R., Santoro, G. E. & Privitera, L. Localization, Topology, and Quantized Transport in Disordered Floquet Systems. *Phys. Rev. Lett.* **123**, 266601 (2019).
- Ippoliti, M. & Bhatt, R. N. Dimensional Crossover of the Integer Quantum Hall Plateau Transition and Disordered Topological Pumping. *Phys. Rev. Lett.* **124**, 086602 (2020).
- Cai, W. et al. Observation of Topological Magnon Insulator States in a Superconducting Circuit. *Phys. Rev. Lett.* **123**, 080501 (2019).
- Zhao, S. K. et al. Probing Operator Spreading via Floquet Engineering in a Superconducting Circuit. *Phys. Rev. Lett.* **129**, 160602 (2022).
- Shi, Y.-H. et al. Quantum Simulation of Topological Zero Modes on a 41-Qubit Superconducting Processor. *Phys. Rev. Lett.* **131**, 080401 (2023).
- Materials and methods are available as supplementary materials.
- Li, J., Chu, R.-L., Jain, J. K. & Shen, S.-Q. Topological Anderson Insulator. *Phys. Rev. Lett.* **102**, 136806 (2009).
- Groth, C. W., Wimmer, M., Akhmerov, A. R., Tworzydło, J. & Beenakker, C. W. J. Theory of the Topological Anderson Insulator. *Phys. Rev. Lett.* **103**, 196805 (2009).
- Meier, E. J. et al. Observation of the topological Anderson insulator in disordered atomic wires. *Science* **362**, 929 (2018).
- Stützer, S. et al. Photonic topological Anderson insulators. *Nature* **560**, 461 (2018).
- Liu, G.-G. et al. Topological Anderson Insulator in Disordered Photonic Crystals. *Phys. Rev. Lett.* **125**, 133603 (2020).
- Wu, Y.-P., Tang, L.-Z., Zhang, G.-Q. & Zhang, D.-W. Quantized topological Anderson-Thouless pump. *Phys. Rev. A* **106**, L051301 (2022).
- Georgescu, I., Ashhab, S. & Nori, F. Quantum simulation. *Rev. Mod. Phys.* **86**, 153 (2014).
- You, J. Q. & Nori, F. Atomic physics and quantum optics using superconducting circuits. *Nature* **474**, 589 (2011).
- Gu, X., Kockum, A. F., Miranowicz, A., Liu, Y.-X. & Nori, F. Microwave photonics with superconducting quantum circuits. *Phys. Rep.* **718**, 1 (2017).
- Cheng, B. et al. Noisy intermediate-scale quantum computers. *Front. Phys.* **18**, 21308 (2023).
- Satzinger, K. J. et al. Realizing topologically ordered states on a quantum processor. *Science* **374**, 1237 (2021).
- Semeghini, G. et al. Probing topological spin liquids on a programmable quantum simulator. *Science* **374**, 1242 (2021).
- Daley, A. J. et al. Practical quantum advantage in quantum simulation. *Nature* **607**, 667 (2022).
- Zhang, X. et al. Digital quantum simulation of Floquet symmetry-protected topological phases. *Nature* **607**, 468 (2022).
- Li, X.-G. et al. Mapping a topology-disorder phase diagram with a quantum simulator, <https://arxiv.org/abs/2301.12138>
- Yan, Z. et al. Strongly correlated quantum walks with a 12-qubit superconducting processor. *Science* **364**, 753 (2019).
- Rice, M. J. & Mele, E. J. Elementary Excitations of a Linearly Conjugated Diatomic Polymer. *Phys. Rev. Lett.* **49**, 1455 (1982).
- Su, W. P., Schrieffer, J. R. & Heeger, A. J. Solitons in Polyacetylene. *Phys. Rev. Lett.* **42**, 1698 (1979).

48. Ke, Y., Qin, X., Kivshar, Y. S. & Lee, C. Multiparticle Wannier states and Thouless pumping of interacting bosons. *Phys. Rev. A* **95**, 063630 (2017).
49. Ivakhnenko, O. V., Shevchenko, S. N. & Nori, F. Nonadiabatic Landau–Zener–Stückelberg–Majorana transitions, dynamics, and interference. *Phys. Rep.* **995**, 1 (2023).
50. Soukoulis, C. M. & Economou, E. N. Off-diagonal disorder in one-dimensional systems. *Phys. Rev. B* **24**, 5698 (1981).
51. Tang, L.-Z., Liu, S.-N., Zhang, G.-Q. & Zhang, D.-W. Topological Anderson insulators with different bulk states in quasiperiodic chains. *Phys. Rev. A* **105**, 063327 (2022).
52. Oka, T. & Kitamura, S. Floquet Engineering of Quantum Materials. *Annu. Rev. Condens. Matter Phys.* **10**, 387 (2019).
53. Koch, J. et al. Charge-insensitive qubit design derived from the cooper pair box. *Phys. Rev. A* **76**, 042319 (2007).
54. Motzoi, F., Gambetta, J. M., Rebentrost, P. & Wilhelm, F. K. Simple Pulses for Elimination of Leakage in Weakly Nonlinear Qubits. *Phys. Rev. Lett.* **103**, 110501 (2009).
55. Mondragon-Shem, I., Hughes, T. L., Song, J. & Prodan, E. Topological criticality in the chiral-symmetric AIII class at strong disorder. *Phys. Rev. Lett.* **113**, 046802 (2014).

Acknowledgements

We thank Yun-Long Su for the helpful discussions and the support from the Synergetic Extreme Condition User Facility (SECUF) in Huairou District, Beijing. Devices were made at the Nanofabrication Facilities at Institute of Physics, CAS in Beijing. This work was supported by the National Natural Science Foundation of China (Grants Nos. 92265207, T2121001, 92365301, T2322030, 12122504, 12274142, 12475017), the Innovation Program for Quantum Science and Technology (Grant No. 2021ZD0301800), the Beijing Nova Program (No. 20220484121), the Natural Science Foundation of Guangdong Province (Grant No. 2024A1515010398), the Nippon Telegraph and Telephone Corporation (NTT) Research, the Japan Science and Technology Agency (JST) [via the Quantum Leap Flagship Program (Q-LEAP), and the Moonshot R&D Grant Number JPMJMS2061], the Asian Office of Aerospace Research and Development (AOARD) (via Grant No. FA2386-20-1-4069), and the Office of Naval Research (ONR).

Author contributions

H.F. and K.X. supervised the project; Y.-R.Z. proposed the idea; Y.L. performed the experiment with the assistance of Y.-H.S. and K.X.; Z.X. fabricated the device with the help of G.-H.L., Z.-Y.M., and D.Z.; Y.L., C.L. and S.-Y.Z. performed the numerical simulations and discussed with Y.-R.Z., Y.-H.S., Tao L., Tong.L., Y.-Y.W., and K.X.; H.L., T.-M.L., C.-L.D., Tong

L., J.-C.Z., G.-H.L., Z.-Y.M., W.-G.M., H.-T.L., Z.-H.L., C.-T.C., K.H., S.P.Z., and Y.T. helped the experimental setup supervised by K.X.; X.S. provided the Josephson parametric amplifiers; Y.-R.Z., F.N., and H.F. gave theoretical explanations; Y.L., Y.-H.S., Y.-R.Z., K.X., and H.F. co-wrote the manuscript, and all authors contributed to the discussions of the results and development of the manuscript.

Competing interests

The authors declare no competing interests.

Additional information

Supplementary information The online version contains supplementary material available at <https://doi.org/10.1038/s41467-024-55343-2>.

Correspondence and requests for materials should be addressed to Zhongcheng Xiang, Kai Xu or Heng Fan.

Peer review information *Nature Communications* thanks the anonymous reviewers for their contribution to the peer review of this work. A peer review file is available.

Reprints and permissions information is available at <http://www.nature.com/reprints>

Publisher's note Springer Nature remains neutral with regard to jurisdictional claims in published maps and institutional affiliations.

Open Access This article is licensed under a Creative Commons Attribution-NonCommercial-NoDerivatives 4.0 International License, which permits any non-commercial use, sharing, distribution and reproduction in any medium or format, as long as you give appropriate credit to the original author(s) and the source, provide a link to the Creative Commons licence, and indicate if you modified the licensed material. You do not have permission under this licence to share adapted material derived from this article or parts of it. The images or other third party material in this article are included in the article's Creative Commons licence, unless indicated otherwise in a credit line to the material. If material is not included in the article's Creative Commons licence and your intended use is not permitted by statutory regulation or exceeds the permitted use, you will need to obtain permission directly from the copyright holder. To view a copy of this licence, visit <http://creativecommons.org/licenses/by-nc-nd/4.0/>.

© The Author(s) 2024